AAS-18-380

STUDYING THE MOTION OF A SPACECRAFT ORBITING AN ASTEROID MODELED AS AN ASYMMETRIC MASS DIPOLE

Leandro F. Brejão,[*] Leonardo B. T. Santos,[†] Diogo M. Sanchez[‡] and Antonio F. B. A. Prado[§]

In this study, the dynamics of a space vehicle in the vicinity of a binary system of asteroids is analyzed by modeling one of the primaries as a rotating mass dipole considered to be in a spin-orbit resonance. Different mass distributions for the binary and for the dipole are considered, as well as different dimensional configurations. Then, the influence of such characteristics on the location of the equilibrium points of the system is studied. The zero velocity curves of the system are also plotted, identifying the regions of forbidden and allowed motion for a spacecraft travelling near the system. Finally, several maps are made showing the lifetimes of orbits as a function of their initial conditions, where the end of the life of an orbit is defined as a collision with any of the bodies or an ejection from the system.

INTRODUCTION

In this study, the dynamics of a space vehicle in the vicinity of a binary system of asteroids is analyzed. In this system, there are two bodies called primaries, with one of them more massive and assumed to be homogeneous and of spherical shape. For the smaller primary, it is assumed to be irregular and modeled by the "Rotating Mass Dipole Model". This model approximates the gravitational potential of an elongated rotating body around an axis perpendicular to its elongation by the gravitational potential of a pair of mass points connected to each other. Such connection is established by an ideal rod, which is rigid and without mass. The length of this dipole is the distance between these two point masses. This model allows the study of the motion of a test particle in the vicinity of systems that are similar to the one described above. Aspects of the surface of the bodies, such as elevations and craters, that affect their mass distribution, are ignored in this model.

Asteroids are in heliocentric orbits within a range that begins within the Earth's orbit and extends beyond the orbit of Saturn, but most of them are located in a region between the orbits of

[*]Master Student, Division of Space Mechanics and Control, National Institute for Space Research - INPE, 12227-010 São José dos Campos, Brazil.
[†]PhD Student, Division of Space Mechanics and Control, National Institute for Space Research - INPE, 12227-010 São José dos Campos, Brazil.
[‡]Post-doctoral Fellow, Division of Space Mechanics and Control, National Institute for Space Research - INPE, 12227-010 São José dos Campos, Brazil..
[§]President of the Board of the Graduate School at INPE in Brazil, National Institute for Space Research - INPE, 12227-010 São José dos Campos, Brazil.

Mars and Jupiter, called the Main Belt of Asteroids. These bodies are believed to be ancient remnants of the early formations of the solar system with more than four billion years of age.

Technological advances in the space sector, in particular in space missions of scientific investigation of the solar system, allowed us to know more about the characteristics of the asteroids. In 1993, the overfly of the Galileo spacecraft around the asteroid Ida showed, for the first time, that such celestial bodies can also have natural satellites. Since then, numerous binary systems of asteroids have been found and cataloged. More than 160 binary systems of asteroids are known nowadays, which is equivalent to 2 to 3% of the bodies of the Main Belt.[1] Several of these bodies migrate from the Main Belt to the proximity of the Sun, and eventually cross the orbits of the inner planets of the solar system. This motion is due to orbital resonances with Jupiter and Saturn. In regions where such resonances occur, an asteroid has its heliocentric orbit disturbed such that it goes to a new orbit, also heliocentric, but with a smaller perihelion.[2] Asteroids that periodically approach Earth are classified as NEAs (Near Earth Asteroids). NEAs are part of a broader category of celestial bodies called NEOs (Near Earth Objects). Such objects, in addition to asteroids, also include comets. Technically, NEAs are asteroids whose perihelion distance is less than 1.3 AU (1 AU is the Astronomical Unit, which is equals to 1.495979×10^8 km).[*] It is also known that there are binary systems of asteroids that approach the Earth and, therefore, are classified as NEAs. There are currently more than 14,000 NEAs known.[**] About 15% of asteroids classified as NEAs are binary systems.[1] Another important feature of asteroids is that, just like any celestial body, such bodies exhibit rotational motion. Asteroids stabilize in uniform rotation on the axis of the largest moment of inertia, regardless of the initial rotation state.[3*]

Several asteroids were object of study or target of space missions. The reasons are: (i) To investigate the chemical composition of these bodies, for the purpose of mining operations of their resources, in particular metallic, which may become scarce on Earth in the future. In addition, the chemical constituents of asteroids are raw materials that can support space exploration activities. In particular, many bodies of the NEAs category can be reached relatively easily, which reduces the cost of transferring rocks and materials to the vicinity of the Earth.[4] (ii) To refine the understanding of the celestial dynamics of these bodies, especially of large asteroids, is important for the development of strategies to prevent their possible collision with Earth.[4] Among the NEAs, there is the subcategory of PHAs (Potentially Hazardous Asteroids). Such bodies exhibit a minimum distance of intersection with the orbit of the Earth less or equal to 0.05 AU. It is estimated that 1,697 asteroids are PHAs for the Earth.[*] For the development of diversion maneuvers of asteroids of the PHAs category, there is a need of space missions in which a vehicle must be able to visit short-term asteroids in order to implant explosive or propellant devices on the surface of such bodies. For this, a detailed understanding of the nature of surfaces of the asteroids is required to predict how these bodies will react to such interventions.[4] (iii) To promote greater knowledge about the origin and formation of the solar system, because asteroids are made of materials that were not incorporated into the planets when the solar system was formed. These bodies exhibit scientific information related to the properties of the early Solar System.[4]

Whatever the purpose of a mission that targets an asteroid, the estimation of the gravitational potential of this object is of fundamental importance for its success.[5] In particular, rotating celestial bodies of irregular shape introduce considerable complexity to the estimation of their

[*] https://cneos.jpl.nasa.gov/faq/#ast

[**] http://neo.jpl.nasa.gov/stats/

gravitational potential.[5] Due to the wide variety of irregular forms of smaller bodies, the spherical harmonic model are not very adequate to be applied to those bodies, because it converge very slowly or even diverge near the surface of the body.[5] Thus, several alternative methods for modeling and estimating the gravitational potential of asteroids have been developed to provide a better understanding of the dynamics of a space vehicle in the vicinity of those deformed bodies. The Polyhedral Method is also an alternative. Due to the high precision of this model, which is based in the geometric form of the central body, it has been widely used in numerous studies to obtain the gravitational field of several asteroids. The accuracy of the approximation of this method depends considerably on the number of faces and vertices used to discretize and represent the geometry of the surface of the body analyzed.[6] The disadvantage of this method is that it is based on previous imaging of the celestial body and a detailed knowledge of its shape is required. Other forms of estimation of the gravitational potential of irregular asteroids include simpler models, like a solid line segment, a dumbbell-shaped body composed of two spheres and a cylinder connecting them and also a rotating mass dipole and other.[7,8,9,10,11] In particular, the mass dipole model was proposed and adopted to approximate the gravitational field of an halter-shaped body.[12,13]

In this study, a mathematical model is established for a test particle that moves around a binary system of asteroids in which one of the bodies is modeled as a rotating mass dipole with spin-orbit resonance. Then, the equilibrium points of this system are studied, as well as their zero velocity curves. Finally, the lifetime of a test particle traveling around the primary body modeled as a dipole is studied, measuring the time that an orbit lasts before colliding with one of the primaries or ends in ejection from the system.

MATHEMATICAL MODEL

It is assumed that the primaries have finite masses. The primary I, of mass m_1, is more massive and presents spherical shape. Primary II, of mass m_2, presents irregular shape. The centroids of primaries I and II, respectively, are denoted by Cp_1 and Cp_2. B is the mass center of the binary, which is adopted as the origin of the sidereal reference system $Bxyz$. The primaries I and II describe circular trajectories around B in the Bxy plane.[14] The radii of the trajectories of the primaries I and II are, respectively, a and b.

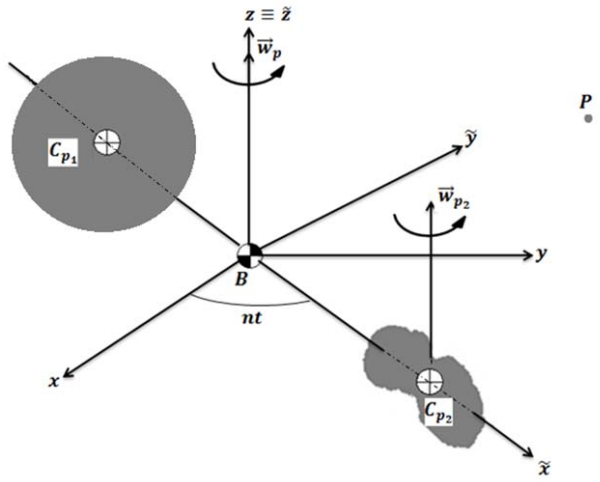

Figure 1. Schematic Representation of the Binary.

Given that $m_1 > m_2$, it follows that $a < b$. It is defined that $l = a + b$ is the distance between the centroids of the primaries. The spacecraft is represented by a test particle P of negligible mass and with motion restricted to the orbital plane of the primaries. The average orbital motion of the primaries is denoted by $\vec{w}_p$ and its magnitude is defined as $\left\|\vec{w}_p\right\| = n$. The irregular primary has an angular velocity $\vec{w}_{p_2}$ of rotation in the plane of its motion, assumed to be constant. In this model, a spin-orbit resonance is considered for this primary, so $\vec{w}_{p_2} = \vec{w}_p$. Figure 1 illustrates the configuration of the binary. The primary I, having spherical shape and homogeneous mass distribution, can be modeled as a mass point denoted by P_1, which coincides with its centroid Cp_1. Due to the irregular shape of primary II, the rotating mass dipole model, composed of two mass points, P_{21} and P_{22}, of masses m_{21} and m_{22}, respectively, is adopted to model this body, such that $m_{21} + m_{22} = m_2$.

Let d be the distance between the poles P_{21} and P_{22}, which is the length of the connecting rod. It is assumed that the distances of P_{21} and P_{22} to the centroid Cp_2 are d_1 and d_2, respectively, such that $d_1 = d_2 = \frac{d}{2}$. Using the spin-orbit resonance configuration, the mass points P_1, P_{21} and P_{22} remain aligned to B at any instant and, to obtain time-independent equations of motion for P, its adopted here the reference system $B\tilde{x}\tilde{y}\tilde{z}$, called the synodic system.[14] The origin of this system is the point B and its movement is assumed to be counterclockwise with respect to $Bxyz$.

The binary parameter is defined as $\frac{m_2}{M} = \frac{a}{l} = \mu$ where $M = m_1 + m_2$ is the total mass of the binary. In analogy, the dipole mass parameter is defined as $\frac{m_{21}}{M} = \mu^*$ and the dipole mass factor, denoted by f, which relates the mass parameters of the binary and the distribution of mass of the dipole, such that $\mu^* = f\mu$ with $0 < f < 1$. It is also considered $d^* = \frac{d}{l}$ as the ratio between the length of the dipole and the distance between the centroids of the primaries. Through this parameterization, the synodic coordinates of the mass points representative of the primary are:

$$\begin{bmatrix} x_1^* & y_1^* \end{bmatrix}^T = \begin{bmatrix} -\mu & 0 \end{bmatrix}^T, \tag{1}$$

$$\begin{bmatrix} x_{21}^* & y_{21}^* \end{bmatrix}^T = \begin{bmatrix} 1-\mu-\frac{d^*}{2} & 0 \end{bmatrix}^T, \tag{2}$$

$$\begin{bmatrix} x_{22}^* & y_{22}^* \end{bmatrix}^T = \begin{bmatrix} 1-\mu+\frac{d^*}{2} & 0 \end{bmatrix}^T. \tag{3}$$

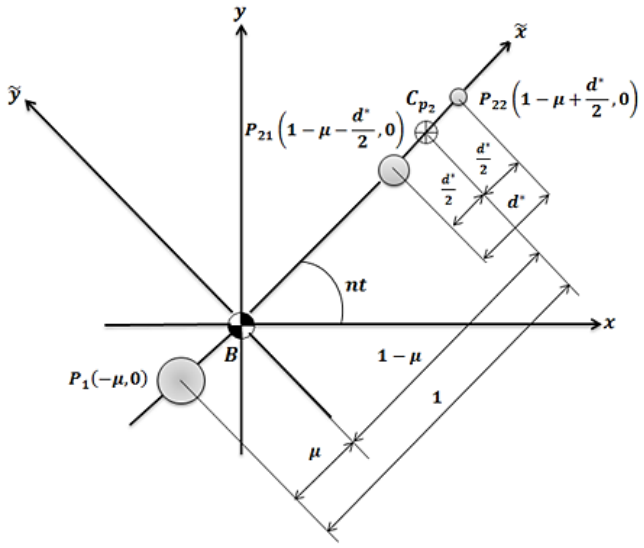

Figure 2. Schematic Representation of the Mass Points Model.

Figure 2 shows the representation of the "Mass Points Model." Consequently, the full potential of the system is of the form:

$$\Omega\left(x^*, y^*\right)=\frac{1}{2}\left[\left(x^*\right)^2+\left(y^*\right)^2\right]+\frac{1-\mu}{r_1^*}+f\,\frac{\mu}{r_{21}^*}+(1-f)\frac{\mu}{r_{22}^*} \tag{4}$$

where the first term is the pseudo-centrifugal potential and the following terms are the gravitational potentials due to P_1, P_{21} and P_{22}, respectively. We also have that x^* and y^* are the dimensionless synodic coordinates of the test particle. In addition, it is easy to see that:

$$r_1^*=\left[\left(x^*+\mu\right)^2+\left(y^*\right)^2\right]^{1/2}, \tag{5}$$

$$r_{21}^*=\left\{\left[x^*-\left(1-\mu-\frac{d^*}{2}\right)\right]^2+\left(y^*\right)^2\right\}^{1/2}, \tag{6}$$

$$r_{22}^*=\left\{\left[x^*-\left(1-\mu+\frac{d^*}{2}\right)\right]^2+\left(y^*\right)^2\right\}^{1/2} \tag{7}$$

are the distances from P to P_1, P_{21} and P_{22}, respectively. Consequently, the equations of motion of the test particle in the synodic system are:

$$\ddot{x}^*-2\dot{y}^*=\Omega_{x^*}\left(x^*, y^*\right)=\frac{\partial}{\partial x^*}\Omega\left(x^*, y^*\right) \tag{8}$$

$$\ddot{y}^*+2\dot{x}^*=\Omega_{y^*}\left(x^*, y^*\right)=\frac{\partial}{\partial y^*}\Omega\left(x^*, y^*\right) \tag{9}$$

RESULTS AND DISCUSSIONS

Based in the model just described, several numerical experiments are made to study the dynamics of the system.

Study of the Equilibrium Points of the System

Taking Equations (8) and (9) and making them equal to zero, we obtain:

$$\Omega_{x^*}\left(x^*, y^*\right) = 0 \tag{10}$$

$$\Omega_{y^*}\left(x^*, y^*\right) = 0 \tag{11}$$

The real solutions of this system of algebraic equations defines a set of points in the plane of motion of the primaries in which there is zero resultant acceleration. Physically, at such points, the centrifugal pseudo-force is balanced by the resulting gravitational force from the mass points P_1, P_{21} and P_{22}. In practical terms, if the test particle, at a given instant, occupy the position of one of these points, the particle will be subject to zero total acceleration, considering the analysis of its dynamics in the synodic frame, so they are equilibrium points. In order to study the variation of the synodic coordinates of the equilibrium points as the parameters vary, simulations were performed for different combinations of values of the parameters μ and d^*, considering a continuous variation of the parameter f in the interval $(0,1)$. In all situations, for each combination of parameters, there are five equilibrium points, three of them collinear and placed along the synodic x-axis (L_1, L_2 and L_3), and two with non-zero synodic ordinate (L_4 and L_5). They are called Lagrange points. In addition to the dynamic equilibrium between the centrifugal pseudo-force and the gravitational resultant on the Lagrange points, it is also necessary to consider the internal competition of the gravitational forces coming from the mass points P_1, P_{21} and P_{22}.

For the collinear Lagrangean point L_3, it is verified that there is no appreciable change in its location, because this is the equilibrium point closest to the primary, so variations in the dipole size and mass has little effects in this point.

Since the collinear Lagrangean points L_1 and L_2 are near the dipole, as the parameter f changes, the location of these points also change. Physically, due to the proximity of these equilibrium points to the dipole, its size and mass distribution impacts in the location of these equilibrium points. It is observed that, using smaller values for the mass parameter μ of the binary, the intervals of variation of the locations of the points L_1 and L_2 as a function of f tend to be closer to the dipole, which location is at the abscissa $1-\mu$. Physically, the smaller the mass parameter of the binary, the smaller the mass of the dipole. Consequently, the gravitational effect of the dipole on the equilibrium points is reduced and the effect of the mass point P_1 becomes more important. In order to preserve the equilibrium conditions for L_1 and L_2, they tend to move to the vicinity of the dipole. In this way, L_1 shows increases in its abscissa, while L_2 has decreases with μ. It is also important to note that the pseudo-centrifugal force does not explicitly depend on the mass parameter of the binary, however, the strength of this force tends to vary

indirectly with the parameter μ,to compensate for the variation of the gravitational forces between the mass points of the system and, in this way, to preserve the equilibrium.

From Figures 3(a) and 3(b), it is noted that L_1 is more sensitive than L_2 to the variation of the binary mass parameter. From Figure 3(a) to Figure 3(b) the mass of the dipole is reduced by one third and, while L_2 presents its variation as a function of f in the same interval at x, we notice that L_1 modifies its range of variation, going to two times closer to the centroid of the dipole than in the previous case shown in Figure 3(a). This is explained by the fact that L_1 has its location between P_1 and the dipole, so the simultaneous effects of the increase of mass of P_1 and the decrease of mass of the dipole, when compared to L_2, are more affected by the distance from the larger primary of the system. Another point is that, the smaller the parameter μ, due to the greater proximity of the points L_1 and L_2 to the dipole, the more sensitive are the locations of these points with f, according to Figures 3(c) and 3(d). The reason for this behavior is that, when μ becomes smaller, the dipole starts to dominate gravitationally the location of the points L_1 and L_2. Thus, for the physical system under study, the smaller the value of the parameter μ, the more significant are the gravitational influences in the mass and distance in the location of the equilibrium points L_1 and L_2 due to the mass point P_1 and the poles P_{21} and P_{22} of the dipole, respectively. In the opposite side, the higher the value of μ, these effects on L_1 and L_2 tend to be distributed to the three mass points of the system.

The locations of the equilibrium points L_1 and L_2 are more sensitive to the variation of the parameter f when larger values are assumed for the parameter d^*. Physically, the greater the value of d^*, the further apart are the poles P_{21} and P_{22}, and the dipole is larger. It makes the positions of the pole P_{21} to be closer to the mass point P_1 for a given value of the parameter μ, while the pole P_{22} increases its distance from P_1. This consequent arrangement of the mass points of the system affects the competition of the gravitational forces from each of them with respect to what was explained before. In general terms, for the given mass parameter μ of the binary, the greater the relative dipole dimension compared to the dimension of the system, the greater the increase of the gravitational effect of P_{21} and P_{22} in terms of the location of the equilibrium points L_1 and L_2 with respect to the gravitational effects associated with P_1. Thus, the larger are the variations in the locations of L_1 and L_2 for a given increment of f and, as a result, the greater the range of possible locations for the equilibrium points.

For each configuration of the parameters μ and d^*, when the parameter f increases, the more massive becomes the pole P_{21} in detriment of the mass reduction of the pole P_{22} of the dipole. As a result of this change in the internal mass distribution of the dipole and to preserve the equilibrium condition for L_1 and L_2, it is observed that the point L_1 tends to move away from the centroid of the dipole, while the point L_2 tends to approach it. On the other hand, considering the reduction of the parameter f, the pole P_{22} presents increment of mass whereas the pole P_{21} decreases its mass and, consequently, L_1 tends to approach the centroid of the dipole while L_2 tries to move away from this point. This behavior is due to the fact that there is a dispute of

gravitational influence between the mass points P_{21} and P_{22}. For fixed values of μ and d^*, as the parameter f changes, there are variations in the intensity of the gravitational forces with respect to the mass of the poles of the dipole. Consequently, there are modifications in the locations of the equilibrium points L_1 and L_2.

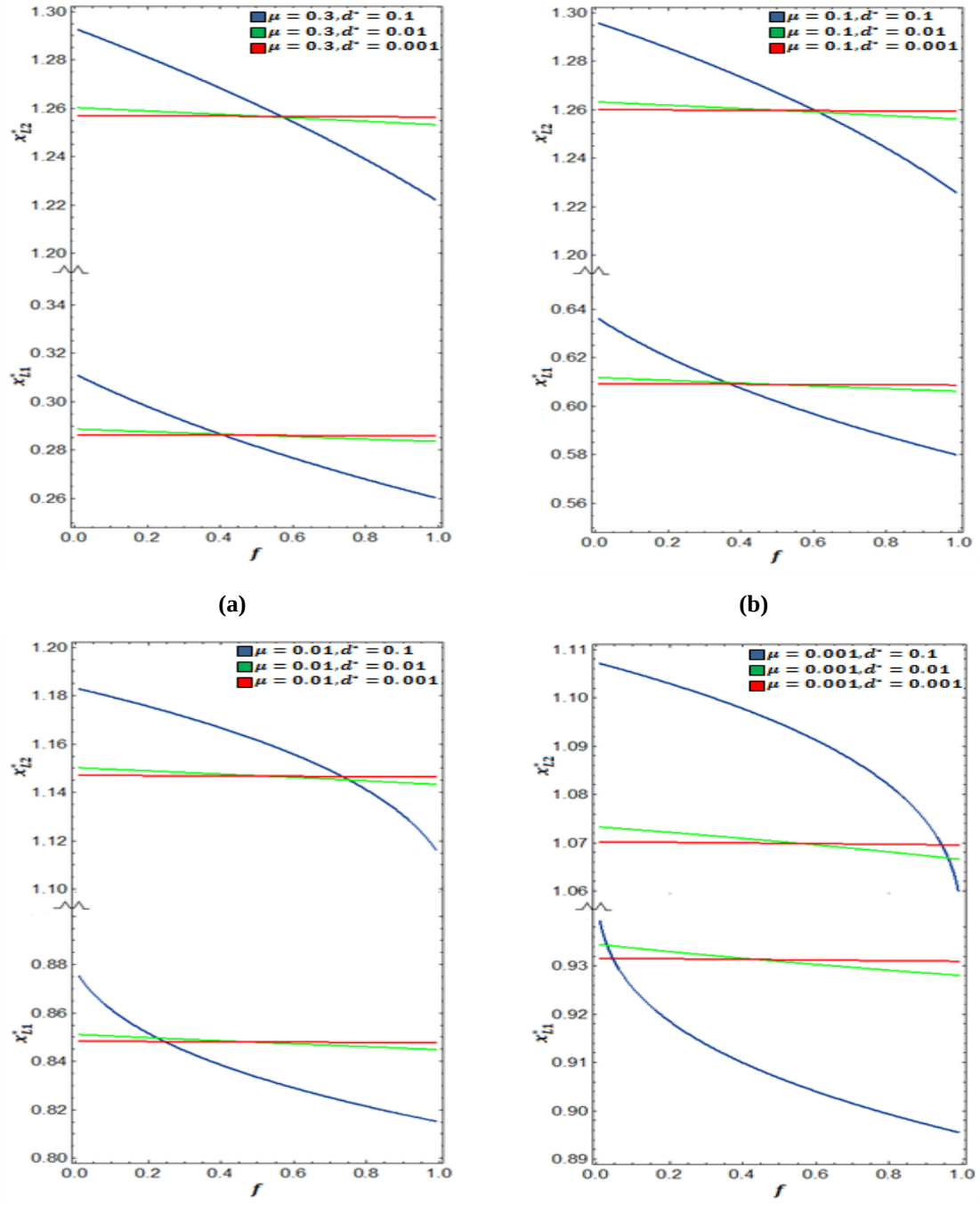

(a) **(b)**

(c) **(d)**

Figure 3. Behavior of the Equilibrium Points.

In general, it can be seen from the above that the dependence of locations of the equilibrium points L_1 and L_2 of the system with the parameters μ, d^*, f occurs simultaneously on two scales: binary, where the parameter μ determines how close or how far L_1 and L_2 are from P_1; dipole scale, where the parameters d^* and f refine the arrangement of the equilibrium points L_1 and L_2 according to the size and internal mass distribution of the dipole, respectively. To quantify the variations of the locations of the equilibrium points, an asteroid system with mass parameter $\mu = 0.1$ and geometric dipole parameter $d^* = 0.1$ was used for the simulations. Three values were used for the parameter f to consider asymmetric cases: $f = 0.25$ and $f = 0.75$ for the mass dipole distribution. They were compared with the symmetric dipole case ($f = 0.5$). We adopted the configuration in which the primaries are two mass points as the reference configuration for the analysis of the locations of the equilibrium points. In the sequence, in Table 1, the locations of the equilibrium points are shown for the symmetric and asymmetric configurations chosen, as well as for the reference configuration.

Table 1. Comparison of the Locations of the Equilibrium Points of the Binary Assuming a Dipole with Different Values of f and the reference.

	$f = 0.25$	$f = 0.5$	$f = 0.75$	Reference
x_{L1}	0.6167710	0.6018982	0.5898750	0.6090351
x_{L2}	1.2825658	1.2669562	1.2483811	1.2596998
x_{L3}	-1.0414106	-1.0416255	-1.0418403	-1.0416098
y_{L1-2-3}	0	0	0	0
x_{L4-5}	0.4043092	0.4010811	0.3978973	0.4000000
y_{L4}	0.8625978	0.8655608	0.8684549	0.8660254
y_{L5}	-0.8625978	-0.8655608	-0.8684549	-0.8660254

Based on Table 1, and in what has been discussed about Figure 3, it can be observed that, in comparison with the reference, the equilibrium points L_1 and L_2 are those that present larger variations in their locations as f varies. From Table 1 it can also be seen that the abscissa of L_1 and L_2, in the symmetrical case, are closer to the abscissa of these points in the reference configuration. The reason for this behavior is the fact that, in the case of the symmetric dipole ($f = 0.5$), its center of mass coincides with the centroid of the dipole, which in the case of the reference is the particle itself, represented by the second primary. As a result, the gravitational influence of a symmetrical dipole on the locations of the points L_1 and L_2 resembles the influence of a single mass point that concentrates the entire mass of the dipole.

For the equilibrium point L_3, it can be seen that the location of this point does not show significant variations with respect to the three parametric cases analyzed and, in addition, the location of L_3 practically do not differ with respect to the reference. Finally, points L_4 and L_5 are studied, considering variations of the mass factor f. The behavior of the variations of the abscissa of these points is similar to what happens for L_1, as discussed in Table 1 and Figure 3, since L_4 and L_5 are also located between the more massive primary and the dipole. Also, according to Table 1, it is possible to notice that the abscissas of L_4 and L_5 in the symmetrical case are closer to the abscissa of these points in the reference configuration, for the same reasons presented for L_1 and L_2. Since the mass distribution of the dipole is made on the axis of the synodic abscissa, there is no mass variation along the synodic ordinates, which explains the small variations of the ordinates of L_4 and L_5 as f varies.

Zero Velocity Curves of the System

The following relation can be obtained for the present problem:

$$\left\|\vec{v}^*\right\|^2 = 2\Omega\left(x^*, y^*\right) - C^* \tag{12}$$

where $\left\|v^*\right\|^2$ is the square of the Euclidean metric norm of the velocity vector of the proof particle P in the dimensionless synodic coordinate system. Equation (12) is called the Jacobi Integral and the integration constant C^* is the Jacobi (dimensionless) constant, which is a first integral of the non-classical motion of the proof particle.[14]

Considering $\mu = 0.1$, $d^* = 0.1$ and mass factor f for the asymmetric cases ($f = 0.25$ and $f = 0.75$) and symmetric ($f = 0.5$) dipoles, the values of the Jacobi dimensionless constant are presented in Table 2, for each equilibrium point of the system. The values of the dimensionless Jacobi constant associated with each equilibrium point for the reference configuration are also presented. From Table 2, it can be seen that, as the mass factor f of the dipole changes, the Jacobi dimensionless constants associated with L_1 and L_2, that is C^*_{L1} and C^*_{L2}, are the ones with the most significant variations. This behavior is due to the fact that, as shown previously, the equilibrium points L_1 and L_2 are immediately adjacent to the dipole. It is also noted that, due to the lower sensitivity to the factor f of the points L_3, L_4 and L_5, the Jacobi dimensionless constants associated with them, C^*_{L3} and C^*_{L4-5}, respectively, exhibit smaller variations compared to C^*_{L1} and C^*_{L2}, as the mass distribution of the dipole is modified. It also happens because L_1 and L_2 are the equilibrium points whose locations on the synodic abscissa are the most sensitive to the variation of f among all the equilibrium points of the system, as shown in Table 2. From the Jacobi dimensionless constant associated to each equilibrium point of the system, considering the three cases presented above for the value of the mass factor f of the dipole, zero velocity curves for the binary system were plotted. Such zero velocity curves are determined by making Equation (12) equal to zero, as follows, for $i = 1,2,..,5$:

$$2\Omega\left(x^*, y^*\right) - C_{Li}^* = 0 \tag{13}$$

Table 2. Jacobi Dimensionless Constant Values Associated with the System Equilibrium Points for the Values of f .

	$f = 0.25$	$f = 0.5$	$f = 0.75$	Reference
C^*_{L1}	3.55619	3.61709	3.67261	3.59695
C^*_{L2}	3.51353	3.47731	3.43748	3.46668
C^*_{L3}	3.09832	3.09965	3.10097	3.09958
C^*_{L4-5}	2.90743	2.90994	2.91243	2.91000

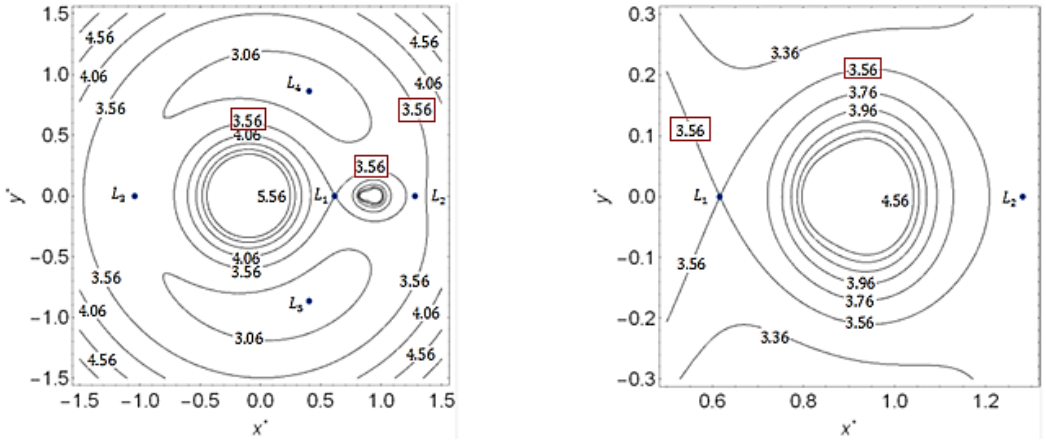

(a) **(b)**

Figure 4: Zero Velocity Curves for the Equilibrium Point L_1 (Indicated by the Red Mark) for $f = 0.25$. In (a) the General Layout and in (b) the Layout Around the Dipole.

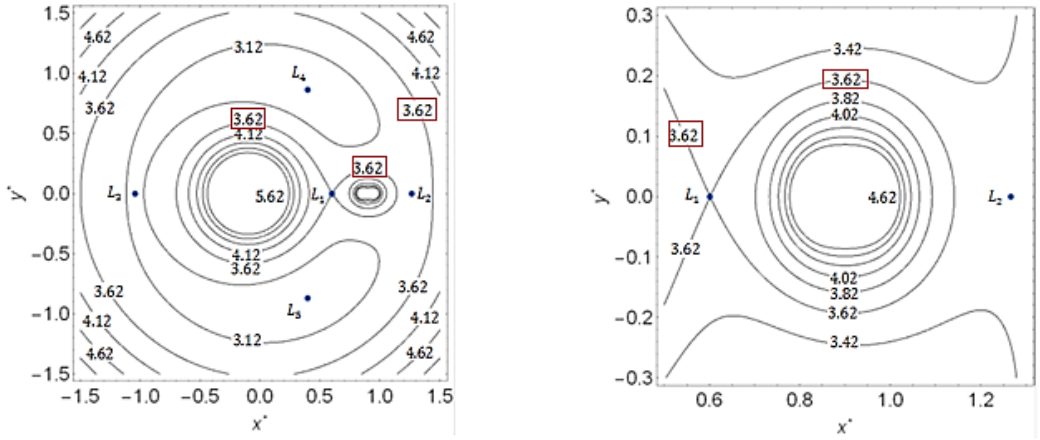

(a) **(b)**

Figure 5: Zero Velocity Curves for the Equilibrium Point L_1 (Indicated by the Red Mark) for $f = 0.5$. In (a) the General Layout and in (b) the Layout Around the Dipole.

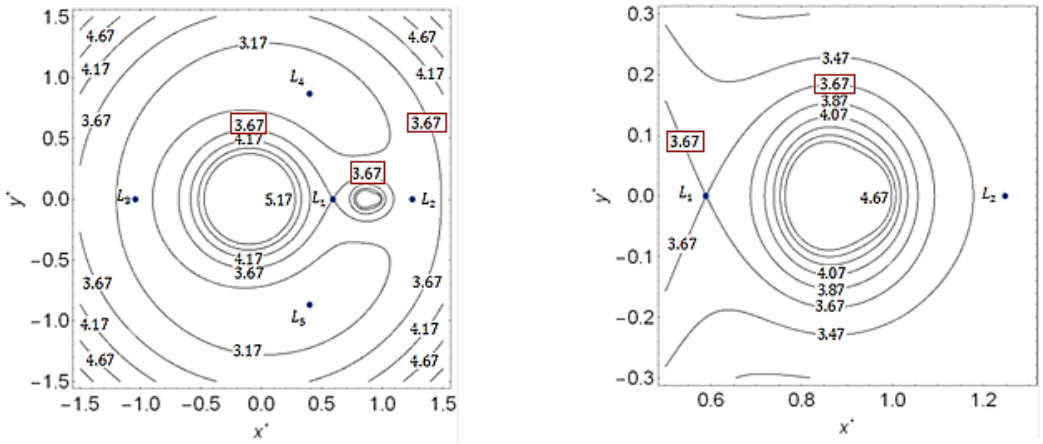

(a) **(b)**

Figure 6: Zero Velocity Curves for the Equilibrium Point L_1 (Indicated by the Red Mark) for $f = 0.75$. In (a) the General Layout and in (b) the Layout Around the Dipole.

Figures 4,5 and 6 (a), (b) show the zero velocity curves associated with C^*_{L1} and their evolution as the dipole mass factor f is varied. These curves intersect at the point of equilibrium L_1 and, for this reason, it is also called the first point of contact. L_1 is the smallest value of the dimensionless specific mechanical energy for the test particle that enables the spontaneous, that is, non-propelled, transfer between the regions surrounding the primary I and the primary II treated. Figures 4 (b), 5 (b) and 6 (b) also show, in greater detail, the plotting of these curves in the vicinity of the mass dipole.

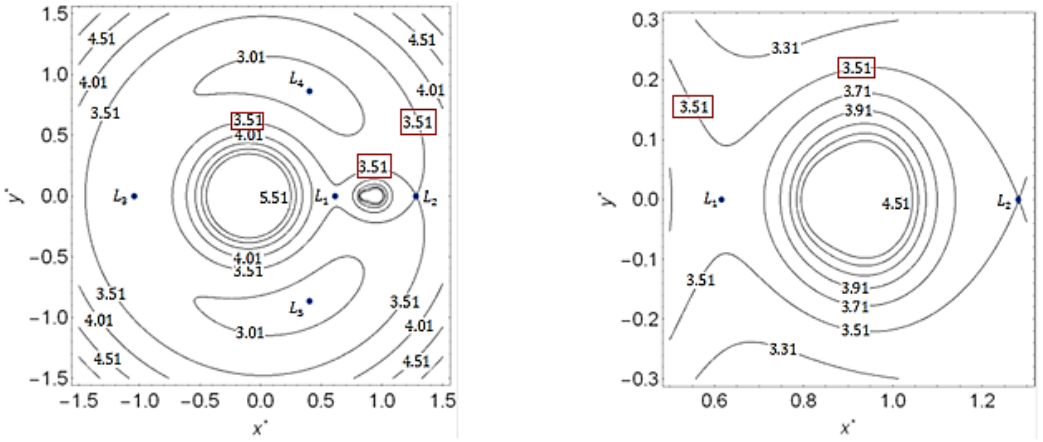

(a) **(b)**

Figure 7: Zero Velocity Curves for the Equilibrium Point L_2 (Indicated by the Red Mark) for $f = 0.25$. In (a) the General Layout and in (b) the Layout Around the Dipole.

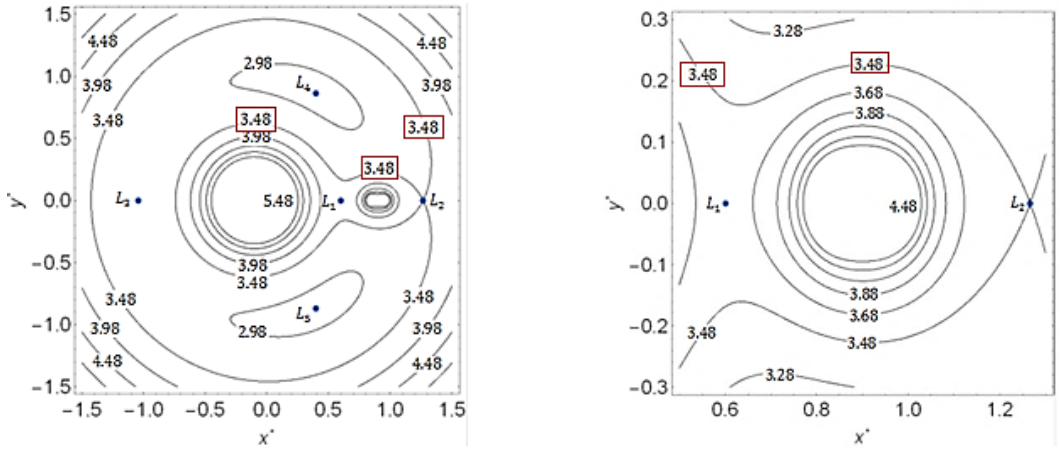

(a) **(b)**

Figure 8: Zero Velocity Curves for the Equilibrium Point L_2 (Indicated by the Red Mark) for $f = 0.5$. In (a) the General Layout and in (b) the Layout Around the Dipole.

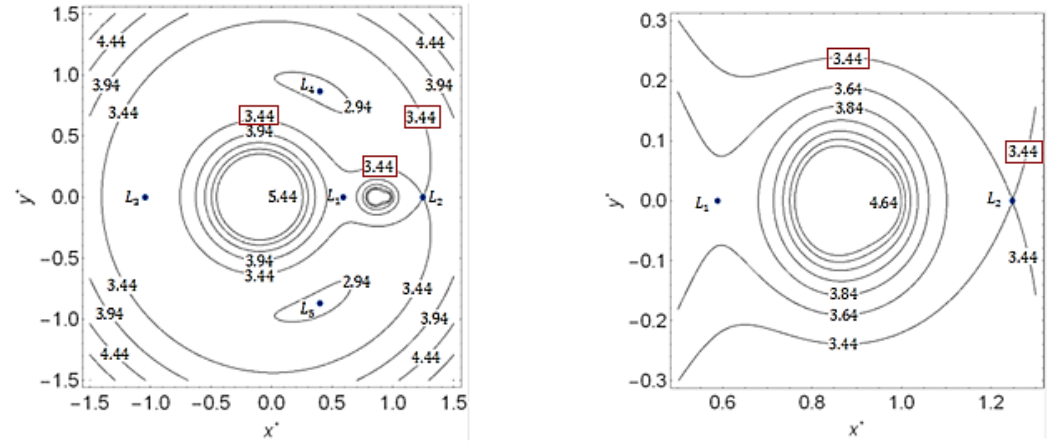

(a) **(b)**

Figure 9: Zero Velocity Curves for the Equilibrium Point L_2 (Indicated by the Red Mark) for $f = 0.75$. In (a) the General Layout and in (b) the Layout Around the Dipole.

When the value of the dimensionless constant of Jacobi assumes the value C^*_{L2}, we have the second point of contact, namely the point of equilibrium L_2, as done for the cases of mass factor f presented in Figures 7 to 9. This point allows a passage for the proof particle to move between the neighborhoods of primaries I and II and infinity, from the primary II. Figures 7(b), 8(b) and 9(b) also show, in greater detail, the plotting of these curves in the vicinity of the mass dipole.

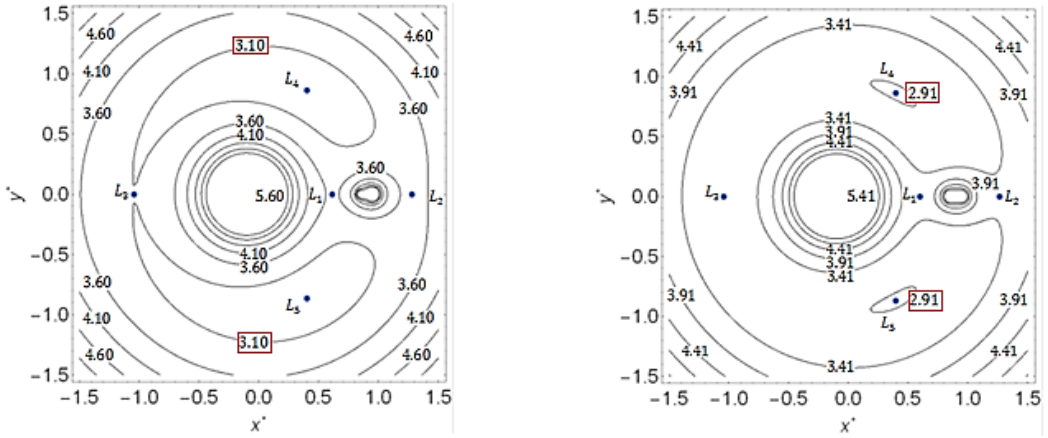

(a) **(b)**

Figure 10: Zero Velocity Curves for the Equilibrium Point L_3 in (a) and Zero Velocity Curves for the Equilibrium Points L_{4-5} in (b) (Indicated by the Red Mark).

When the dimensionless constant of Jacobi assumes the value C^*_{L3}, we have the third point of contact, namely the point of equilibrium L_3, considered for the cases of mass factor f presented. This point allows, similarly to what occurs for L_2, to have a passage where the test particle can go from the neighborhoods of the primaries I and II to infinity. By reducing the value of the dimensionless constant of Jacobi to the point where it takes the value C^*_{L4-5}, there is a considerable reduction of regions spontaneously forbidden for the motion of the test particle. Consequently, the regions that energetically allow spontaneous movement of the third body of the system become larger. Under these conditions, the regions energetically forbidden for the test particle are located in the vicinity of the equilibrium points L_4 and L_5. Due to the smaller variations of the Jacobi dimensionless constant for the points L_3, L_4 and L_5 with the variation of the mass factor f of the dipole, no significant changes in the zero velocity curves of the system was observed for the values of f used here. In this way, in Figure 10 we present the general plot of these curves for the Jacobi dimensionless constants, for each value of the mass factor f, associated with C^*_{L3} and C^*_{L4-5}.

The test particle, in its motion, can reach the equilibrium points of the binary. In the case of the points L_1, L_2 and L_3 the particle reaches them with zero velocity, because these points belong to the zero velocity curves and with zero acceleration, by the dynamic equilibrium condition used to determine these equilibrium points. Consequently, for the test particle to pass through the energy gap defined by L_1, L_2 and L_3, it is necessary that it has an excess of energy in its movement. As a result of these points being equilibrium points of the unstable type, small perturbations of the system itself on the test particle are sufficient for the energy increment required for the transposition of L_1, L_2 and L_3. However, the equilibrium points L_4 and L_5, which have linear stability, define regions in their neighborhood where, if the test particle occupies them, it is not possible that the particle leaves them spontaneously. To avoid these regions, a spacecraft would need to use propulsion.

Survival Time of a Spacecraft Around the Dipole

The development of missions directed at irregular celestial bodies, such as asteroids, requires the study and quantification of the stability and navigability of space vehicles in orbits close to such bodies.[3] When planning a space mission where a vehicle will approach a celestial body, it is necessary to analyze its length of stay around the body to ensure that the mission can be completed. Due to disturbances of other celestial bodies and the irregular shape of bodies such as asteroids, such analysis is even more important, especially to determine the initial conditions for the movement of the vehicle which can lead to collisions or ends in the gravitational ejection from the system. Considering the parameterization of the problem in the inertial frame, besides the gravitational forces exerted by the mass points P_1, P_{21} and P_{22} of the system, the force associated with the solar radiation pressure on the space vehicle will also be considered, as shown in the following equations of movement:

$$\ddot{\xi}\left(t^*\right) = -\frac{(1-\mu)\left[\xi\left(t^*\right)+\mu\cos\left(t^*\right)\right]}{r_1^3} - \frac{f\mu\left[\xi\left(t^*\right)-\left(1-\mu-\frac{1}{2}d^*\right)\cos\left(t^*\right)\right]}{r_{21}^3} - \frac{(1-f)\mu\left[\xi\left(t^*\right)-\left(1-\mu+\frac{1}{2}d^*\right)\cos\left(t^*\right)\right]}{r_{22}^3} - P_{rad\xi} \tag{14}$$

$$\ddot{\eta}\left(t^*\right) = -\frac{(1-\mu)\left[\eta\left(t^*\right)+\mu\sin\left(t^*\right)\right]}{r_1^3} - \frac{f\mu\left[\eta\left(t^*\right)-\left(1-\mu-\frac{1}{2}d^*\right)\sin\left(t^*\right)\right]}{r_{21}^3} - \frac{(1-f)\mu\left[\eta\left(t^*\right)-\left(1-\mu+\frac{1}{2}d^*\right)\sin\left(t^*\right)\right]}{r_{22}^3} - P_{rad\eta} \tag{15}$$

where $\xi = \frac{x}{l}$ and $\eta = \frac{y}{l}$ are the dimensionless inertial coordinates of the spacecraft e $t^* = nt$. Also:

$$r_1 = \sqrt{\left[\xi\left(t^*\right)+\mu\cos\left(t^*\right)\right]^2 + \left[\eta\left(t^*\right)+\mu\sin\left(t^*\right)\right]^2} \tag{16}$$

$$r_{21} = \sqrt{\left[\xi\left(t^*\right)-\left(1-\mu-\frac{1}{2}d^*\right)\cos\left(t^*\right)\right]^2 + \left[\eta\left(t^*\right)-\left(1-\mu-\frac{1}{2}d^*\right)\sin\left(t^*\right)\right]^2} \tag{17}$$

$$r_{22} = \sqrt{\left[\xi\left(t^*\right)-\left(1-\mu+\frac{1}{2}d^*\right)\cos\left(t^*\right)\right]^2 + \left[\eta\left(t^*\right)-\left(1-\mu+\frac{1}{2}d^*\right)\sin\left(t^*\right)\right]^2} \tag{18}$$

The terms $P_{rad\xi}$ and $P_{rad\eta}$ are the components of acceleration due to the solar radiation pressure. It is known that the acceleration of the solar radiation pressure is given by:[15,16,17]

$$P_{rad} = -C_r \frac{A}{m} P_s \left(\frac{r_0}{R} \right)^2 \hat{r} \tag{19}$$

where C_r is the radiation pressure coefficient that depends on the reflectivity of the vehicle. In this study the value of C_r = 1.5 was used. P_s is the solar radiation pressure in the Earth's orbit and it is approximately 4.55 x10^{-6} N/m². The term r_0 is the Sun-Earth distance and R is the Sun-spacecraft distance. It is assumed that $\hat{r}$ is the radial unit distance in the direction of the Sun relative to the vehicle. A is the area of the spacecraft exposed and illuminated by the Sun and m is the mass of that vehicle. In the simulations the values of 1 m² for A and 100 kg for the mass were adopted, resulting in the vehicle area-to-mass ratio A/m = 0.01 m² / kg.[18] The reason for considering the effect of the solar radiation pressure in this study is due to the fact that, depending on the relative position of the spacecraft with respect to the Sun at the initial conditions, the solar radiation pressure tends to push the vehicle against the dipole. The closer the vehicle is to the dipole in its initial position, the faster it will tend to collide with the primary II and thus the solar radiation pressure can reduce the life of the vehicle in its mission.[18]

For the analysis of the time spent by the spacecraft around the dipole, it is useful to construct grids of initial conditions for the vehicle's motion.[18] Considering the binary, such grids establish initial conditions (for t = 0) of semi-major axis and eccentricity for an osculating Keplerian orbit of the vehicle around the dipole-shaped body. This initial osculating Keplerian orbit is considered, for all cases, as having two return points (closed orbits) and to be in the plane of movement of the primaries. For the purposes of simulations, both direct and retrograde orbits are considered for the spacecraft around the dipole. The grids of the initial conditions are referenced to the center of mass of the dipole. The space vehicle has the eccentricity of its Keplerian osculating orbit initiated at zero and verified until e = 0.99. Its major half-axis varies from 500 meters with respect to the centroid of the dipole up to the Hill's radius for this body, with consideration of 50 meters more as extra margin.[17] This procedure is performed for a binary with a mass parameter $\mu = 0.1$and considering a dipole whose geometric characteristic parameter is $d^* = 0.1$. The cases of asymmetric dipole ($f = 0.25$ and $f = 0.75$) and symmetric dipole ($f = 0.5$) are analyzed. From the osculating Keplerian orbital elements, the initial position and velocity for the vehicle are obtained in sidereal Cartesian coordinates. Then, Equation (24) and Equation (25) are integrated. The total integration time adopted here is one year, which corresponds to approximately 500 orbital periods of the binary. An integrator Runge-Kutta 7/8 was used with time step of 0.01 canonical unit.

As a criteria for evaluating the results, orbits are investigated in which the spacecraft survives for at least 500 orbital periods of the primaries (integration period). In this study, a collision occurs with the most massive primary when the initial position of the vehicle is less than or equal to the radius of this body**.** In addition, if the position of the vehicle at a given time is less than the dimensions of the less massive primary (diameter 500 meters on the x axis and 250 meters on the y axis), the vehicle collides with this primary. It is also considered that there is a gravitational ejection of the vehicle with respect to the binary when the initial position of the vehicle is greater than 30 times the distance between the primaries. The understanding of these perturbations on a test particle in the vicinity of the binary system is of fundamental importance for the

determination of regions of stability around the system in which one can have families of orbits with larger durations. However, the stability of these regions can lead to the accommodation of dust clouds or particle agglomerates around the binary, since the smaller the mass of a celestial body, the less intense is its gravitational field. The detection of dust around the system, which per image cannot be observed, suggests that the families of orbits located in these regions should be avoided to preserve the integrity of the space vehicle. In contrast, unstable regions may have little or no dust. In this way, families of orbits in such regions are safer options for the vehicle.[20,21,22]

For the total time of integration of 500 orbital periods of the system, it was observed that there is no survival of orbits, having collisions of the vehicle with some of the bodies of the binary or gravitational ejection from the system. For $f = 0.25$ it was observed that, in the retrograde case, the spacecraft is more likely to collide with the more massive primary. From the initial semi-major axis of approximately 500 meters to a range of eccentricities from 0 to approximately 0.85. In the direct case, the vehicle is more likely to be gravitationally ejected from the system. This phenomenon occurs for the initial semi-major axis greater than about 650 m and in an approximate interval of eccentricities from 0 to 0.8, both in the retrograde and direct cases, for values smaller than the initial semi-major axis discussed and in the eccentricity intervals adopted, the spacecraft would collide with the primary modeled as a dipole. For $f = 0.5$ it was observed that, in both the retrograde and direct cases, the initial conditions grid indicates the predominance of collisions of the spacecraft with the most massive primary. In particular, in the direct case, for initial semi-major axis larger than 1,200 meters and eccentricity between 0 and 0.4, gravitational ejection of the vehicle occurred. In the case of $f = 0.75$, it was observed the tendency of collisions of the spacecraft with the most massive primary of the system. Therefore, new simulations were made considering only the first 30 days of simulation.

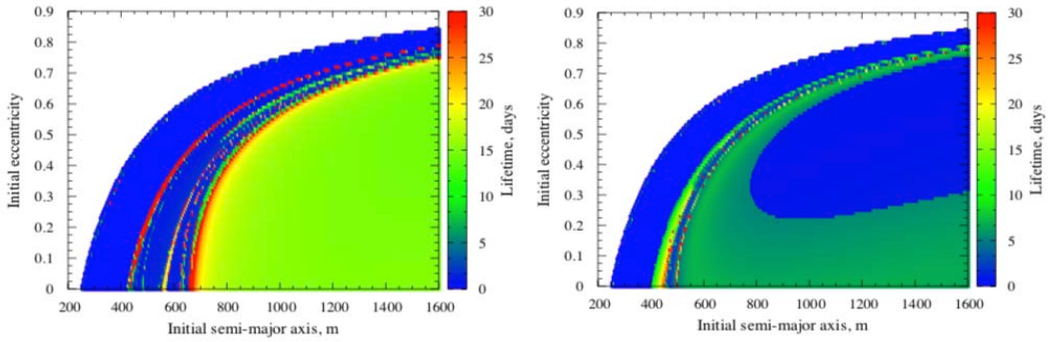

(a) **(b)**

Figure 11: Grids of Initial Conditions in Semi-major Axis and Eccentricity for $f = 0.25$ and Considering Integration Time of 30 Days. In (a) the Direct Case and in (b) the Retrograde Case.

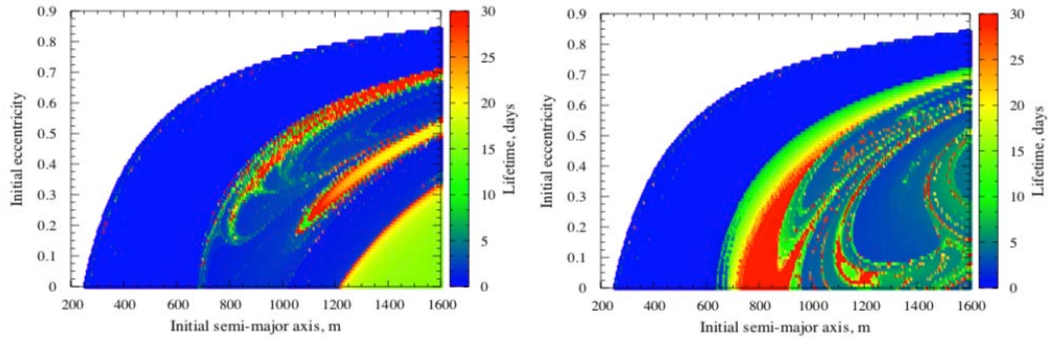

(a) **(b)**

Figure 12: Grids of Initial Conditions in Semi-major Axis and Eccentricity for $f = 0.5$ and Considering Integration Time of 30 Days. In (a) the Direct Case and in (b) de Retrograde Case.

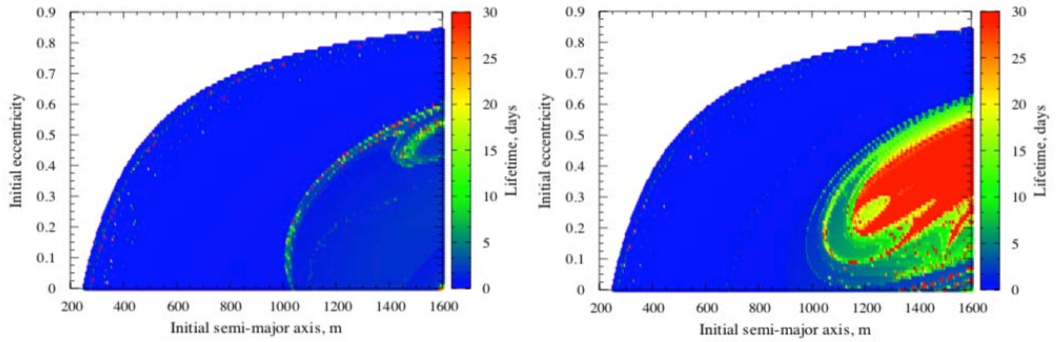

(a) **(b)**

Figure 13: Grids of Initial Conditions in Semi-major Axis and Eccentricity for $f = 0.75$ and Considering Integration Time of 30 Days. In (a) the Direct Case and in (b) de Retrograde Case.

Figures 11(a) and 11(b) show grids of the initial condition for the system under study considering $f = 0.25$. It is clear that, in the direct case, the spacecraft has a spectrum of orbits of longer duration around the central body (dipole) in comparison with the retrograde case, although the region in which such orbits are found may contain dust and, therefore, should be avoided. From Figures 12(a) and 12(b), for $f = 0.5$, it can be seen that the spacecraft has a larger spectrum of longer orbits around the dipole for the retrograde case, compared to the direct case. In the retrograde case, such orbits are arranged with initial conditions of semi-major axis between 700 and 900 meters with respect to the centroid and, for eccentricities between 0 and 0.5, for the direct case, the longest orbits for the vehicle occur for the semi-major axis greater than 800 meters in a set of eccentricities between around 0.2 and 0.7. Figures 13(a) and 13(b) show that, for $f = 0.75$, the spacecraft also has a larger range of longer-lasting orbits in the retrograde case compared to the direct case. In the retrograde case it is verified that the orbits of longer durations occur for values of semi-major axis above 1,200 meters, approximately, and in a range of eccentricities between 0.1 and 0.5. From the figures presented above it can be observed that the variation of the eccentricity and semi-major axis of the grids of initial conditions is due to two reasons: the mass factor of the dipole and the inclination of the orbital plane of the vehicle with respect to the plane of motion of the primaries. For low values of the dipole mass factor (as

$f = 0.25$), where the most massive pole of the dipole is P_{22}, it is observed that the largest survival times of the vehicle around the dipole is mostly influenced by the inclination of the orbital plane of the vehicle. For larger dipole mass factors (such as $f = 0.75$), the most massive pole of the dipole is P_{21} and it is permanently oriented to the most massive primary, due to spin-orbit resonance. Consequently, in the orbital stretch between P_1 and P_{21} there will be a greater gravitational dispute over the vehicle compared to the opposite asymmetric case.

CONCLUSION

In this work we studied the dynamics of a spacecraft in the vicinity of a binary system in which one of the primaries, in this case the least massive, was modeled as a mass dipole with rotation in spin-orbit resonance.

The behavior of the distribution of the equilibrium points of the binary was studied as a function of the canonical parameters μ, d^* and f. In general terms, the lower the mass parameter μ of the binary and the greater its geometric parameter d^*, the closer to the pole P_{21} of the dipole will be the point of equilibrium L_1, while L_2 gets closer to the pole P_{22} of the dipole. Consequently, these points of equilibrium will be more sensitive in their location on the x axis of the synodic reference system by varying the mass factor f of the dipole. The equilibrium points L_4 and L_5 present slight variations with the parameters studied. Such variations are even smaller in their synodic ordinates given the non-existence of mass distribution along the axis and synodic in the dipole, according to the model used here. The equilibrium point L_3, because it is close to the most massive point-mass of the system P_1, does not show any appreciable variation of its synodic abscissa by varying the canonical parameters of the model. Then, the Jacobi dimensionless constants for each equilibrium point were determined considering the case $\mu = 0.1$ and $d^* = 0.1$ with f varying between 0 and 1, excluding the extremes of this interval. Based on these values, the zero velocity curves were plotted. The spontaneous passage of the vehicle from the oval of the most massive primary to the dipole oval (and vice versa) occurs easily in the case where $f = 0.25$, since the gravitational dispute between points-mass neighbors to L_1 (first point of contact), namely, P_1 and P_{21}, is less intense than in cases of larger f. It has also been observed that the spontaneous passage of the spacecraft from the dipole oval to the outside by means of L_2 (second contact point) is facilitated in the case where $f = 0.75$ and, therefore, the pole P_{22} is less massive exerting less gravitational attraction in this region. Similarly, the spontaneous passage of the spacecraft between the oval of the most massive primary and the outer one through L_3 (third point of contact) practically does not change with f because it is far from the dipole.

Finally, grids of initial conditions for the spacecraft were studied in terms of semi-major axis and eccentricity for osculating Keplerian orbits around the dipole, taking it as the center of the orbital motion. It has been found that, depending on the mass distribution of the dipole, direct or retrograde orbits can have a longer duration. For lower f factor ($f = 0.25$) it was observed that direct orbits have a longer lifetime around the dipole in comparison with retrograde orbits, for the same initial conditions of semi-major axis and eccentricity. For larger f factor ($f = 0.75$), retrograde orbits are the ones that present larger lifetimes. For this reason, since retrograde orbits are not spontaneous and can be used by a vehicle around the dipole, depending on the initial

conditions chosen and the mass distribution of the dipole, these orbits are good choices to be used by a mission.

ACKNOWLEDGMENTS

The authors wish to Express their appreciation for the support provided by grants #2016/14665-2, 2016/18418-0, 2016/24561-0, 2014/22295-5, 2013/07174-4, 2018/00059-9 from São Paulo Research Foundation (FAPESP). We also thank the financial support from the National Council for the Improvement of Higher Education (CAPES) and the National Council for Scientific and Technological Development (CNPq)

REFERENCES

[1] K. J. Walsh. “Asteroids with Satellites: Inventory, Properties, and Prospects for Future Discoveries”. Earth Moon Planet 105, 193–199, 2009.

[2]R. Dvorak, “The Role of Resonances in Astrodynamical Systems”, 2008.

[3]D. J. Scheeres, B. G. Williams and J. K. Miller. “Evaluation of the Dynamic Environment of an Asteroid: Applications to 433 Eros”. Jouranal of Guidance, Control and Dynamics, Vol. 23, No. 3, 2000.

[4]I. A. Crawford.“Asteroids in the Service of Humanity”, 2013.

[5]P. Y. Cui and D. Qiao. “The Present Status and Prospects in the Research of Orbital Dynamics and Control Near Small Celestial Bodies”. Theor. Appl. Mech. Lett. 4(1), 1–14, 2014.

[6]X. Zeng, H. Baoyin and J. Li. “Updated Rotating Mass Dipole with Blateness of One Primary (I): Equilibria in the Equator and their Stability”. Astrophys Space Sci361:14, 2016.

[7]A. Elipe, M. Lara. “A Simple Model for the Chaotic Motion Around (433) Eros”.JAS, 51, 391, 2003.

[8]H. W. Yang, S. Li and C. Xu.“A Particle-Linkage Model for Non-Axisymmetric Elongated Asteroids”.2018.

[9]K. Gozdziewski. “Nonlinear Stability of the LagrangianLibration Points in the Chermnykh Problem”. Celestial Mechanics and Dynamical Astronomy, 70, 41, 41–58,1998.

[10]Broucke R. A. and Elipe, A. The Dynamics of Orbits in a Potential Field of a Solid Circular Ring. Advances in the Astronautical Sciences, v. 119, n.3, p. 3017-3036, 2004.

[11]Broucke, Roger A; Prado, AFBA. Orbits Around an Elongated 3D-Object. Advances in the Astronautical Sciences, v. 119, n.3, p. 3037-3060, 2004.

[12]S. V. Chermnykh.“Stability of Libration Points in a Gravitational Field”. 1987.

[13]A. Kokoriev, A. Kirpichnikov, S. N., Vest. Leningrad Univ. 1, 75, 1988.

[14]V.Szebehely. “Theory of Orbits, The Restricted Problem of Three Bodies”. New York: Academic Press, 1967.

[15]O. Montebruck, E. Gill. “Satellite Orbits: Models, Methods, and Applications”.Springer, Berlin, 2000.

[16]G. Beutler. “Methods of Celestial Mechanics”, vol II: Application to Planetary System. Geodynamics and Satellite Geodesy.Springer, Berlin, 2005.

[17]B. Y. P. L. Masagoet al.: Adv. Space Res. 57, 962, 2016.

[18]L. B. T. Santos, A. F. B. A. Prado and D. M. Sanchez. “Lifetime of a Spacecraft Around a Synchronous System of Asteroids Using a Dipole Model”. Astrophys Space Sci , 2017.

[19]R. A. N. Araujo, O. C. Winter, A. F. B. A. Prado and R. Vieira Martins.Mon. Not. R. Astron. Soc. 391, 675, 2008.

[20]R. A. N. Araujo, O. C. Winter, A. F. B. A. Prado and A. Sukhanov. Mon. Not. R. Astron. Soc. 423, 3058 , 2012.

[21]R. A. N. Araujo, O. C. Winter and A. F. B. A. Prado. Mon. Not. R. Astron. Soc. 153, 1143, 2015.

[22]V. M. Gomes, R. de Cássia Domingos. "Studying the lifetime of orbits around Moons in elliptic motion." Computational and Applied Mathematics, Vol. 35, Nr. 3, 653-661, 2016.